

# Long-Range Ordered Self-Assembly of Novel Acrylamide-Based Diblock Copolymers for Nanolithography and Metallic Nanostructure Fabrication

Je Gwon Lee, Yeon Sik Jung, Sung-Hwan Han, Kwan-Mook Kim, and Yang-Kyoo Han\*

Bottom-up pattern formation at the nanoscale regime has been the focus of enormous research efforts for the past few decades.<sup>[1–4]</sup> In particular, the directed self-assembly (DSA) of block copolymers (BCPs) has shown great promise for sub-20 nm lithography due to advantages including high resolution, scalability, cost-effectiveness, and compatibility with conventional fabrication processes for integrated circuits.<sup>[5–12]</sup> Previous studies have demonstrated that non-regular pattern generation, sub-5 nm resolution, and extensive degree of tunability in pattern dimensions can be achieved using the DSA processes.<sup>[13–16]</sup> In contrast, other alternative techniques such as electron beam lithography, nanoimprint lithography (NIL), and extreme ultraviolet (EUV) lithography have practical challenges in the aspects of throughput and cost.<sup>[17]</sup>

A major barrier toward the widespread use of the DSA technique has been a trade-off among the desirable properties of resulting self-assembled patterns: high resolution, long-range ordering, low defect density, high etch selectivity, perpendicular alignment, and easy pattern transfer onto a substrate. To generate well-defined lithographic patterns, various BCP materials have been developed. For example, polystyrene-*block*-poly(methyl methacrylate) (PS-PMMA) has been the most widely studied DSA polymer owing to its high etch selectivity between the two blocks, the capability of perpendicular alignment, and a rapid and facile assembly process.<sup>[17]</sup> However, its limited resolution and poor long-range ordering, which stem from its relatively low Flory–Huggins interaction parameter, are limiting factors for its applications.<sup>[7]</sup> Polystyrene-*block*-poly(ethylene oxide) (PS-PEO) and polystyrene-*block*-poly(vinyl pyridine) (PS-PVP) BCPs show long-range ordering, low defect density, and extremely high resolution,<sup>[14,18]</sup> however, their

insufficient etch selectivity hampers their adoption in lithographic processes.

In this paper, we report the unusual self-assembly behaviors of a novel poly(p-dodecylphenylacrylamide)-*block*-poly(methyl methacrylate) (PDOPAM-PMMA) BCP, which is composed of a crystalline and hard PDOPAM block, and an amorphous and soft PMMA block.<sup>[19]</sup> Interestingly, the bulk PDOPAM-PMMA BCP with a cylindrical morphology exhibits microdomains with an atypical square-symmetry. This new BCP also offers diverse advantages for their applications in nanolithography compared to conventional BCP materials. First, PDOPAM-PMMA shows exceptional long-range ordering over a 10 μm scale without relying on guiding templates. Second, the etch-rate difference, otherwise known as the etch selectivity, between the two constituent blocks under UV exposure enables facile pattern transfer to an underlying substrate for lithography applications. Nanoscale patterns with good aspect ratio (1.5–2.0) were fabricated on a silicon oxide substrate via simple UV, reactive ion etching (RIE), and O<sub>2</sub> plasma etching procedures. Third, the PDOPAM block can be selectively decorated using various metallic salts, yielding highly uniform metallic lines, dots, and mesh nanostructures. Combining above characteristics, the novel PDOPAM-PMMA BCP that is designed, synthesized, and processed in this work can contribute to resolve the current issues mentioned above and hold great potential as a next-generation lithography technique.

We synthesized PDOPAM-PMMA, a new soft-hard hybrid BCP via a reversible addition fragmentation chain transfer (RAFT)<sup>[20]</sup> polymerization technique using hard, crystalline DOPAM and soft, amorphous MMA monomers. DOPAM monomer with good crystallinity was first synthesized by reacting p-dodecylphenyl amine with acryloyl chloride and purified at specific conditions to produce a single crystal.<sup>[21]</sup> The X-ray diffraction analysis for the single-crystal monomer confirms that it has a monoclinic structure. The three dimensional structure of the DOPAM single crystal was constructed from the crystallographic data (Supporting Information, Table S1 and S2) using a molecular mechanics program (SPARTAN '08), as shown in Figure 1. The crystallinity of the DOPAM is mostly reserved in the PDOPAM block and yields a crystalline structure, which is supported by the DSC thermograms of the PDOPAM-PMMA diblock copolymers (Supporting Information, Figure S1). For systematic observation of the self-assembly behaviors of PDOPAM-PMMA BCP, several BCP samples with different volume fractions and molecular weights (MWs) were prepared. The volume fraction of the PDOPAM block was adjusted in a range of 0.41 to 0.73 (Supporting Information, Scheme S1, Figure S1 and S2, and Table S3). The self-assembly

Dr. J. G. Lee,<sup>[+]</sup> Prof. S.-H. Han, Prof. Y.-K. Han  
Department of Chemistry  
Hanyang University  
222 Wangsimni-ro, Seongdong-gu  
Seoul, 133–791, Korea  
E-mail: ykhan@hanyang.ac.kr

Prof. Y. S. Jung  
Department of Materials Science and Engineering  
Korea Advanced Institute of Science and Technology (KAIST)  
291 Daehak-ro, Yuseong-gu, Daejeon 305–701, Korea

Prof. K.-M. Kim  
Department of Chemistry and Nano Science, Ewha Womans University  
52 Ewhayeo-dae-gil, Seodaemun-gu, Seoul, 120–750, Korea

[+] Present address: Corporate R&D, LG Chem, Ltd., 104–1, Moonji-dong, Yuseong-gu, Daejeon, 305–738, Korea

DOI: 10.1002/adma.201305186



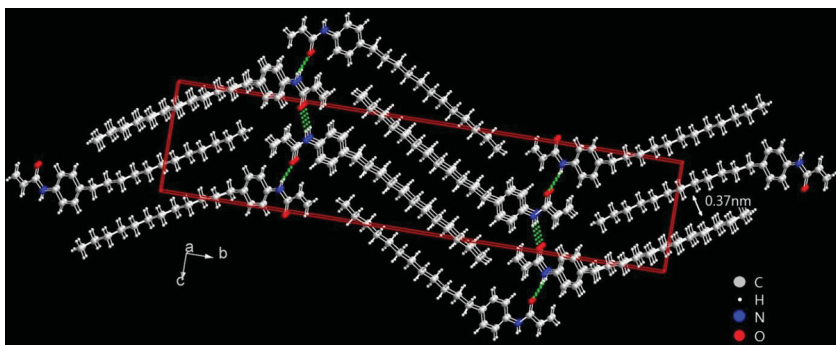


**Figure 1.** Three-dimensional structure of the single crystal of the new acrylamide-type monomer DOPAM. The dotted green line denotes the intermolecular hydrogen bonding (bond distance:  $2.046 \pm 0.010 \text{ \AA}$ ) between the amide groups in each layer. The distance between the benzene groups ( $3.653 \pm 0.017 \text{ \AA}$ ) in the same layer is the same as that of well known  $\pi\text{-}\pi$  interaction.

was performed under the mixture vapor of tetrahydrofuran (THF) (good solvent for both blocks) and cyclohexane with an optimized mixing ratio of 8/2 (v/v). PDOPAM and PMMA are slightly soluble and insoluble in cyclohexane, respectively. Thus, the addition of more cyclohexane (almost nonsolvent) in the mixed solvent can control the vapor pressure of THF and the swelling ratio of the BCP during self-assembly. The self-assembled morphologies were quenched by the rapid removal of solvent molecules from the BCP films, and were confirmed by atomic force microscopy (AFM), scanning electron microscopy (SEM), and X-ray scattering (Supporting Information, Figure S3).

Before discussing the advantages of PDOPAM-PMMA for nanolithography, we report its intriguing morphology. When the film thickness is sufficiently large ( $>100 \text{ nm}$ ), the M1BD41 BCP (weight fraction of PDOPAM,  $f_{\text{PDOPAM}} = 41\%$ ) showed cylindrical microdomains aligned in parallel with the Si wafer substrate containing a native oxide layer, as shown in Figure 2a,b. The SEM images were obtained by selectively staining the PDOPAM block with RuO<sub>4</sub>, and thus the PDOPAM regions appear much brighter than PMMA. Interestingly, the cylinders clearly present a four-fold symmetry (Figure 2c), which is contrary to the traditional BCP theories as well as the numerous experimental results showing that cylindrical microdomains of a diblock copolymer generally have a hexagonal symmetry.<sup>[22,23]</sup> The average diameter and center-to-center spacing of the cylindrical microdomains were 20 nm and 40 nm, respectively. Another BCP with  $f_{\text{PDOPAM}} = 55\%$  (M1BD55) also showed a similar arrangement of cylinders with square symmetry (Figure 2d,e and Supporting Information, Figure S4a–c), confirming that BCPs with a wide composition range exhibit the unusual morphology with four fold symmetry. Cylindrical nanostructures with uniform square symmetry and uniform hexagonal symmetry were formed when

$f_{\text{PDOPAM}}$  was between 41–55% and over 66%, respectively, and arrangements of mixed symmetries were obtained for intermediate compositions (56–65%). When the thickness of the BCPs was smaller than the center-to-center spacing ( $<40 \text{ nm}$ ), they showed monolayer in-plane cylindrical morphologies (Supporting Information, Figure S4d). In addition, we observed that the BCPs with  $f_{\text{PDOPAM}}$  of over 60% are always perpendicularly oriented to the wafer substrate. The cylinders oriented perpendicularly to the substrate showed a mixed arrangement of square and hexagonal symmetries, as can be seen in Figure 2f,g. The formation of square arrays from an unconfined A-B diblock copolymer has not previously been reported

in either experimental or theoretical studies.<sup>[22]</sup> Previously, formation of square patterns has been accomplished using A-B-C triblock terpolymers<sup>[24]</sup> or a mixture of two diblock copolymers linked by hydrogen-bonding<sup>[25]</sup> or dense chemical templates defined by e-beam lithography to constrain the BCP micro-domains.<sup>[26]</sup> This study reports, for the first time, that cylindrical microdomains with a square symmetry can be obtained from a pure diblock copolymer without imposing any spatial confinement. At this point, the formation mechanism of this unusual morphology is not clear, however, we speculate that combination of  $\pi\text{-}\pi$  interaction of the benzene rings, inter- and intramolecular hydrogen-bonding between the amide groups, and van der Waals forces between the long alkyl chains linked to the benzene ring in the side chain of the crystalline PDOPAM block<sup>[19]</sup> may attribute to the four fold symmetry morphology.

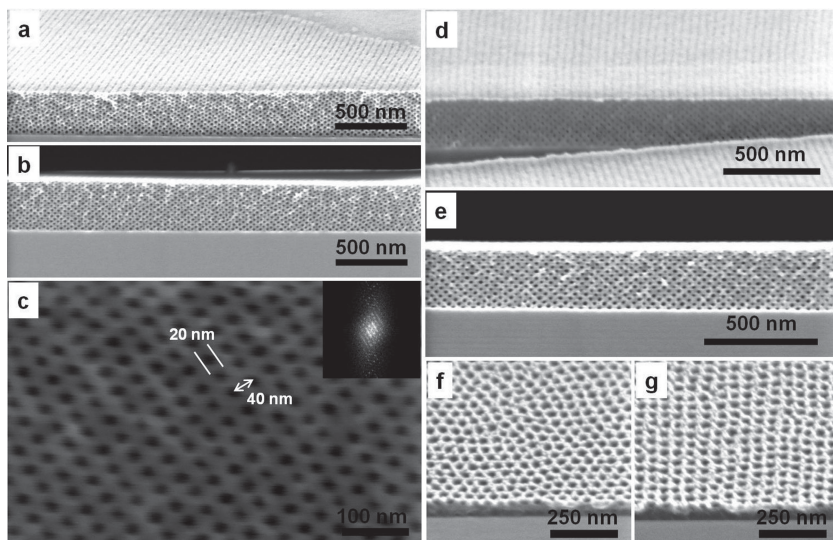


**Figure 2.** 60° and 90° tilted cross-sectional SEM images of: a,b) M1BD41 and d,e) M1BD55 BCP films with a thickness of 300 nm after solvent annealing and RuO<sub>4</sub> staining. c) Higher-resolution image of (b). When the BCP film thickness is over 100 nm and the PDOPAM composition is within a range of 41–55%, horizontally arranged cylinders of PMMA having a square symmetry were observed. f,g) 60° tilted SEM images of M2BD65 thin film with a thickness of 35 nm after solvent annealing, UV etching, and O<sub>2</sub> plasma etching. The out-of-plane cylinders showed a mixed arrangement of (g) square and (f) hexagonal symmetries.

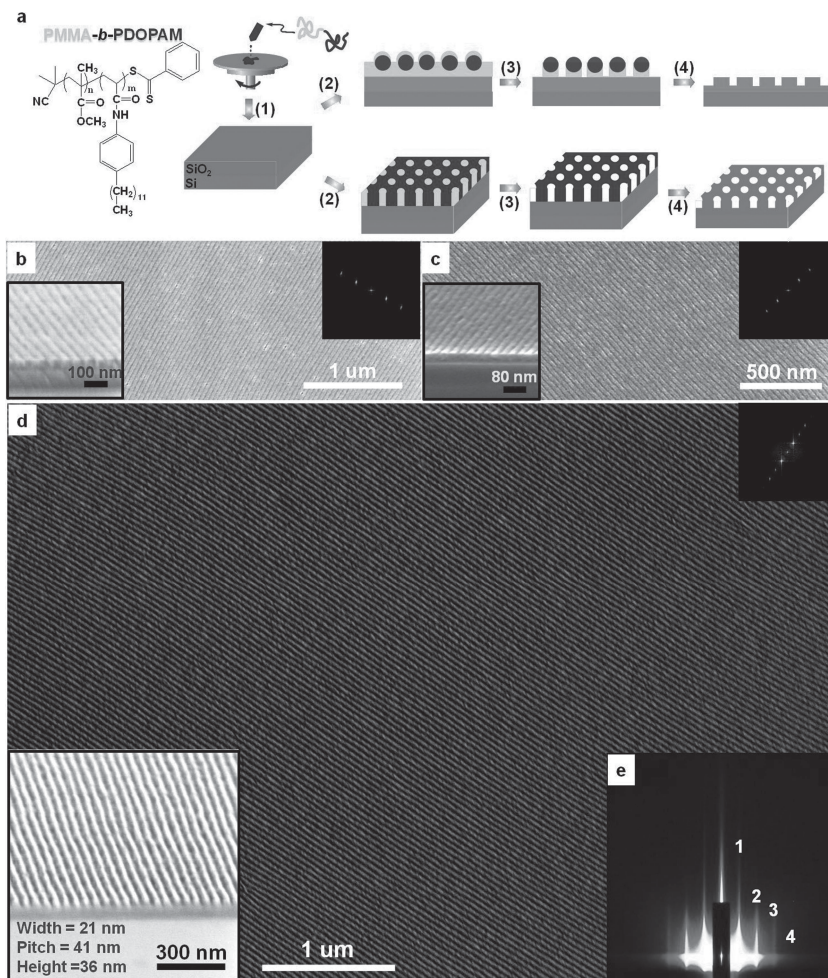


**Figure 3.** a) Schematic representation of the nanofabrication process: (1) spin coating of PMMA-*b*-PDOPAM on a  $\text{SiO}_2$ (100 nm)/Si wafer, (2) formation of highly long-range ordered nano patterns via solvent annealing, (3) selective removal of PMMA by UV etching, (4) fabrication of nano patterns on a silicon oxide template after RIE and  $\text{O}_2$  plasma etching. b,c) Top-view SEM images of (b) M3BD47 ( $MW = 37 \text{ kg/mol}$ ,  $f_{\text{PDOPAM}} = 47\%$ ) and (c) M4BD48 ( $MW = 20.9 \text{ kg/mol}$ ,  $f_{\text{PDOPAM}} = 48\%$ ) thin films after solvent annealing,  $\text{RuO}_4$  staining, and UV etching. d) Top-view SEM image of  $\text{SiO}_2$  nanowires fabricated from M3BD47 thin film by RIE and  $\text{O}_2$  plasma treatment. e) GISAXS pattern of  $\text{SiO}_2$  nanowires showing several diffraction peaks, which indicates good long-range orientational order and uniform periodicity.

Currently, more in-depth analyses and theoretical investigations are underway and will be published elsewhere.

Newly synthesized PDOPAM-PMMA exhibited desirable properties for nanolithography. Figure 3a schematically illustrates a simple procedure to fabricate line or hole pattern on the substrates, which involves: i) spin-coating, ii) pattern formation via self-assembly, iii) selective removal of PMMA by UV etching, and iv) pattern transfer onto the underlying silica layer via reactive ion etching (RIE) and  $\text{O}_2$  plasma etching. Self-assembled PDOPAM-PMMA on a  $\text{SiO}_2$ (100 nm)/Si wafer exhibited exceptional long-range ordering and minimal defect density. In addition, moderate etch selectivity (ca. 2:1) between PDOPAM and PMMA under UV radiation and high RIE resistance of PDOPAM enabled a simple pattern transfer via UV etching and RIE while maintaining the resolution of the nanopatterns.

An example pattern of the self-assembled BCP (M3BD47, MW = 37 kg/mol,  $f_{\text{PDOPAM}} = 47\%$ ) with an in-plane cylindrical morphology (Supporting Information, Figure S5) is shown in Figure 3b. The average line width and pitch were 21 nm and 41 nm, respectively. The SEM image shows that long-range ordered, defect-free patterns are uniformly formed with a correlation length of over 7  $\mu\text{m}$ , which is confirmed by the aligned clear dot patterns in the fast Fourier transform (FFT) image (Figure 3b, inset). The estimated line edge roughness is 2.89 nm as shown in Supporting Information, Figure S6. The line width and pitch of the aligned patterns can be adjusted by tuning the molecular weight (MW) of the BCPs. As presented in Figure 3c, the reduction of MW to 20.9 kg/mol (M4BD48) decreased the line width and pitch to 13 nm and 25 nm, respectively. These pattern sizes, ranging from 21 to 13 nm, satisfy the design rule for next-generation semiconductor fabrication nodes. The exceptional long-range ordering was also observed for the perpendicularly oriented BCP with a cylindrical morphology (Supporting Information, Figure S7). The AFM image (Figure 4a) of the self-assembled BCP (M3BD63) with  $f_{\text{PDOPAM}}$  of 63% and MW of 53.6 kg/mol reveals well-ordered microdomain structures over a large area ( $>4 \mu\text{m}^2$ ) with uniform six-fold symmetry. The top-down and tilted-view SEM images obtained after UV treatment on the self-assembled pattern for selective etching of PMMA show that well-defined nanopores with a depth of 38 nm are uniformly produced (Figure 4b,c). This structure is also supported by the clear FFT patterns in the insets and the GISAXS pattern with hexagonal symmetry (Figure 4d). The average diameter and the center-to-center spacing were estimated to be 25 nm and 45 nm, respectively.

The outstanding degree of long-range ordering is likely attributed to the large Flory-Huggins segmental interaction parameter ( $\chi$ ) of the BCP as well as the crystalline nature of the PDOPAM block. It has been shown that a BCP with a large  $\chi$  value generates patterns with a low defect density and a large correlation length.<sup>[14,27]</sup> The  $\chi$  value of a BCP is proportional to the difference of the surface energy between two constituent polymers. Surface-tension measurements using the Zisman method<sup>[28]</sup> show that the PDOPAM block has extremely low surface tension ( $\gamma = 6.25 \text{ dyne/cm}$ , Supporting Information, Figure S8). The surface tensions of PS and PMMA are 40.7 dyne/cm and 41.1 dyne/cm, respectively.<sup>[29]</sup> These values suggest a much larger  $\chi$  value for PDOPAM-PMMA compared with that of commonly studied PS-PMMA. In addition, a larger correlation length ( $\xi$ ) of the self-assembled patterns tends to yield a smaller defect density ( $D$ ) due

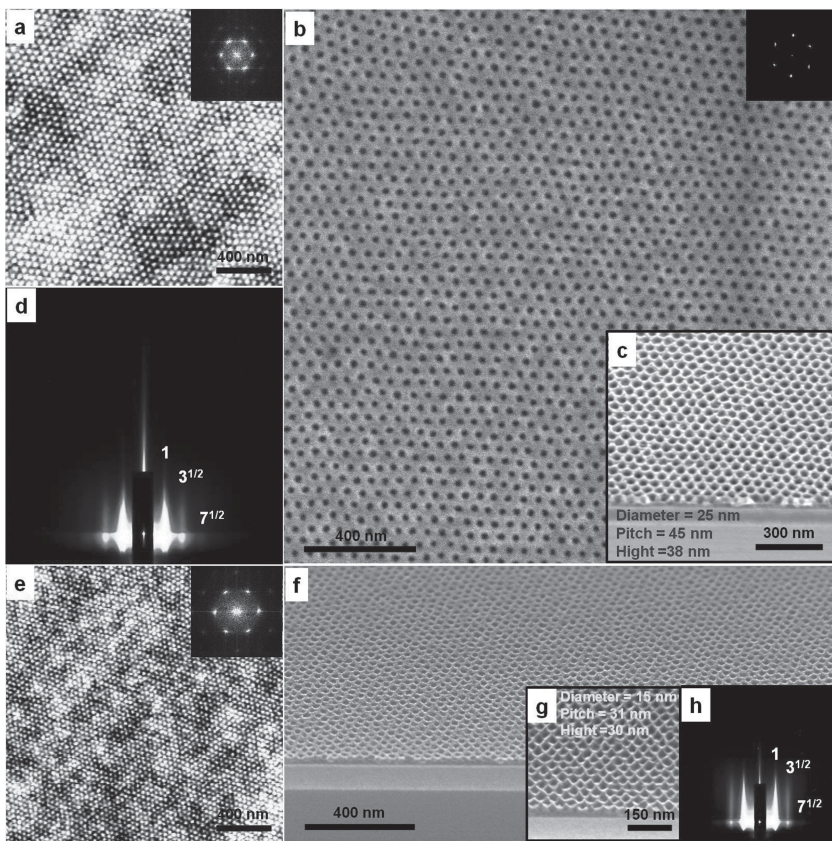


**Figure 4.** AFM images of: a) M3BD63 ( $MW = 53.6 \text{ kg/mol}$ ,  $f_{\text{PDOPAM}} = 63\%$ ) and e) M4BD63 ( $MW = 29.4 \text{ kg/mol}$ ,  $f_{\text{PDOPAM}} = 63\%$ ) films after solvent annealing. b) Top-view SEM image of M3BD63 thin film; f)  $60^\circ$  tilted cross-sectional SEM image of M4BD63 after solvent annealing,  $\text{RuO}_4$  staining, and UV etching. c,g)  $45^\circ$  tilted cross-sectional SEM images of  $\text{SiO}_2$  nanoholes fabricated from M3BD63 (c) and M4BD63 (g) templates by UV etching, RIE, and  $\text{O}_2$  plasma etching. d,h) GISAXS patterns of  $\text{SiO}_2$  nanoholes fabricated from M3BD63 (d) and M4BD63 (h) templates show several diffraction peaks, which indicates good long-range orientational order and uniform periodicity.

to the relation of  $[D \sim \xi^{-2}]$ .<sup>[30]</sup> Considering the much smaller  $\xi$  (50–200 nm) for unguided PS-PMMA, the patterns from PDOPAM-PMMA are predicted to have a much lower defect density.

The moderate etch selectivity and RIE resistance of the new BCP enabled successful transfer of the self-assembled nano-patterns onto a  $\text{SiO}_2(100 \text{ nm})/\text{Si}$  wafer and yielded nanopatterns with good aspect ratio via simple UV, RIE and  $\text{O}_2$  plasma etching steps: PMMA was selectively etched during UV irradiation (Supporting Information, Figure S9 shows line-patterned PDOPAM template films) and the remaining PDOPAM blocks served as a good etch mask for the pattern-underlying materials during RIE (Figure 3d shows  $\text{SiO}_2$  nanoline and space patterns). The etch selectivity of 2:1 for PDOPAM-PMMA is lower than those (>10:1) of Si-containing BCPs such as polystyrene-*b*-polydimethylsiloxane (PS-*b*-PDMS). However, the moderate etch selectivity of PDOPAM-PMMA was sufficient to yield the excellent pattern transfer results due to the high etch resistance of PDOPAM. The FFT pattern in the inset of Figure 3d and the clearly resolved grazing-incidence small-angle X-ray scattering (GISAXS) pattern with high-order peaks,

which is shown in Figure 3e, confirm the uniformity of the nanoscale features over a macroscopic area. The dimension (width = 21 nm, pitch = 41 nm) of the silica nanopatterns was consistent with those of BCP patterns before the pattern transfer, confirming the excellent reliability of the BCP patterns as an etch mask. We also fabricated nanohole patterns on a  $\text{SiO}_2$  thin film using perpendicularly oriented BCPs with a cylindrical morphology (Figure 4c,g). Since the MW of M4BD63 ( $MW = 29.4 \text{ kg/mol}$  and  $f_{\text{DOPAM}} = 63\%$ ) was tuned to be lower than that of M3BD63 ( $MW = 53.6 \text{ kg/mol}$  and  $f_{\text{DOPAM}} = 63\%$ ), M4BD63 exhibited a smaller feature size (diameter = 15 nm, height = 30 nm, and pitch = 31 nm) than M3BD63 (diameter = 25 nm, height = 38 nm, and pitch = 45 nm), as presented in Figure 4e,h. These results show that nanoscale hole patterns with a high aspect ratio (1.5–2.0) can be attained from the novel BCPs without using a neutral brush treatment. This approach is very useful and reliable for patterning underlying materials.<sup>[31]</sup>

We observe that the orientation and position of the microdomain structures can be readily controlled by using guiding templates. As shown in Supporting Information, Figure S10–S13, the BCP nanostructures were uniformly aligned in topographic trench templates with a depth of 100 nm and widths of 1, 2, and 5  $\mu\text{m}$ , where the templates were fabricated by KrF optical lithography. The measured feature sizes and pitches of the patterns assembled in the trenches were identical to those of the patterns on flat substrates. Figure 5d–f

shows the SEM images of the  $\text{SiO}_2$  nanostructures such as nanowires and nanoholes on guiding templates obtained by employing the BCP patterns as etch masks for plasma etching. The size and pitch of the nanowires and nanoholes were easily tunable by adjusting the MWs of the BCPs. The dimension and spacing of the self-assembled nano patterns (Figure 5a–c) were well maintained after the pattern transfer onto the  $\text{SiO}_2$  films, as shown in Figure 5g,h. These results suggest that low-cost optical lithography techniques can be easily combined with the nanolithography technique reported in this paper.

Self-assembled PDOPAM-PMMA is useful not only for nanolithography<sup>[19]</sup> but also for bottom-up fabrication of metallic nanostructures.<sup>[32]</sup> The amide groups in PDOPAM and transition metal ions form complexes in a neutral solution, and therefore, metallic nanostructures can readily be created by simple incorporation of metallic ions onto the nano patterned PDOPAM blocks remaining after UV irradiation. In particular, the neutral reaction conditions enabled fabrication of Ag nanostructures such as nanowires or nanomeshes, which has not been possible using conventional methods. As can be seen in

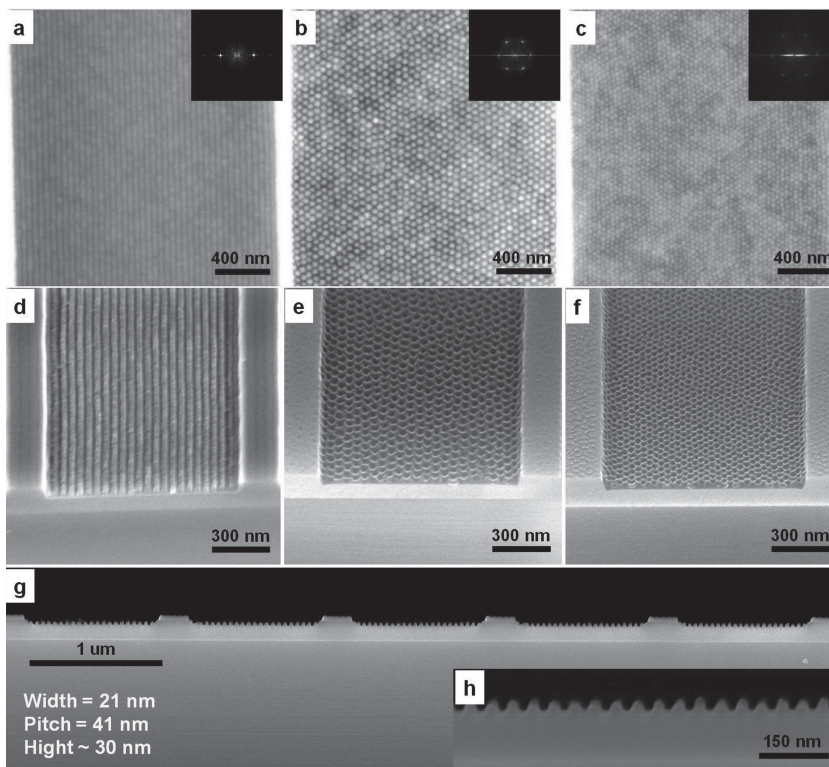


**Figure 5.** AFM images of: a) M3BD47, b) M3BD63, and c) M4BD63 thin films assembled on a 2 μm-wide topographic trench template with a 100 nm-thick SiO<sub>2</sub> layer after solvent annealing. The trench templates were fabricated by KrF optical lithography. d) 45° tilted cross-sectional SEM image of SiO<sub>2</sub> nanowires (width = 21 nm; pitch = 41 nm) fabricated on a 1 μm-wide topographic trench template using the M3BD47 BCP patterns as an etch mask for RIE and O<sub>2</sub> plasma etching. e,f) 45° tilted cross-sectional SEM images of SiO<sub>2</sub> nanoholes fabricated on a 1 μm-wide topographic trench template using the M3BD63 (e) (diameter = 25 nm; pitch = 45 nm) and M4BD63 (f) (diameter = 15 nm; pitch = 31 nm) BCP patterns as etch masks for RIE and O<sub>2</sub> plasma etching. g,h) 90° tilted cross-sectional SEM images of the SiO<sub>2</sub> nanowires prepared using the M3BD47 BCP. These microscopy images confirm the excellent reliability of the pattern-transfer process. h) Higher-resolution image of (g).

**Figure 6.** various metallic nanowires and nanomeshes were successfully formed after immersing the PDOPAM patterns in aqueous solutions of metallic salts followed by O<sub>2</sub> plasma etching, which removes the organic polymer components, and then short thermal reduction under an Ar/H<sub>2</sub> atmosphere, which eliminates oxygen and leave the metal nanostructures.<sup>[32]</sup> For example, Pt, Fe, Co, Pd, Au, and Ag nanowires with an average thickness and diameter of 21 nm and a periodicity of 41 nm were uniformly produced using this method. We also successfully fabricated Pt, Fe, and Ag nanomesh structures with an average pore size of 15–19 nm, a center-to-center spacing of 31 nm. The uniform nanowires and nanomeshes are well characterized by the GISAXS patterns and the X-ray photoelectron spectroscopy (XPS) data, as shown in Supporting Information, Figure S14 and S15, respectively. In particular, this method simply and conveniently generates Ag nanostructures, as PDOPAM easily adsorb metallic ions in a neutral solution. In contrast, previous methods employ acidic solutions containing poly(vinylpyridine) as a counter cation of metallic anions.<sup>[33]</sup> With the conventional preparation procedures, it is impossible to produce silver-based nanowires and nanomeshes

due to their acidic reaction condition. Ag nanomeshes are potentially highly useful as transparent and conducting electrodes that exploit surface plasmonic effects.<sup>[34]</sup> Significant enhancement of transparency in the visible range can be achieved by optimizing the size and spacing of nanoholes via control of the MW of the suggested BCP. In addition to the solution-based metal incorporation, we expect that other vapor or gas-phase pattern-transfer techniques such as sequential infiltration synthesis can also be employed for the fabrication of various oxide nanostructures in a highly controllable manner.<sup>[35]</sup>

To summarize, we report the novel and versatile self-assembly characteristics of PDOPAM-PMMA BCPs to overcome the general limitations of conventional BCPs used for DSA. Simple solvent annealing of the BCPs on a substrate generated nano-lithographic patterns with long-range ordering and minimal defect density. The nanoscale features were readily transferred to an underlying material owing to sufficient etch selectivity between PDOPAM and PMMA under UV radiation and high RIE resistance of PDOPAM. The patterned BCPs were also used as a scaffold for reliable incorporation of various inorganic components to form diverse functional nanostructures. In particular, the neutral reaction conditions enabled fabrication of Ag nanostructures using the self-assembled nano patterns for the first time. These findings suggest that this new BCP is a universal and practical candidate for successful implementation of sub-20 nm DSA processes.

## Experimental Section

**Synthesis of DOPAM Monomer and its Single-Crystal Structure:** Detailed synthetic procedure and crystallographic data (crystal system = monoclinic; space group =  $P2_1/c$  (No.14)) of the PDOPAM single crystal can be found in the Supporting Information (Table S1 and S2).<sup>[21]</sup>

**Synthesis of PMMA-*b*-PDOPAM Diblock Copolymer (M3BD47):** A PMMA-RAFT macroinitiator (0.45 g, 0.023 mmol), DOPAM (0.732 g, 2.32 mmol), AIBN (2.54 mg, 0.015 mmol), and benzene (3.79 mL) were placed into a 10 mL Schlenk flask fitted with a rubber septum and purged with nitrogen for 30 min to remove air. The pink-colored reaction mixture was immersed in a silicone oil bath preheated to 70 °C. The turbid solution became clear and transparent within a few minutes. The clear solution was stirred at 70 °C under a nitrogen atmosphere to conduct polymerization. The polymer solution in benzene was sampled by a syringe in specific time intervals for a GPC analysis. After 72 h, the polymerization was terminated by the addition of a large amount of THF (5 mL). The polymerization mixture was precipitated with excess methanol (250 mL) to yield a novel soft-hard diblock copolymer, PMMA-*b*-PDOPAM, as a pale yellow solid. The crude diblock copolymer was re-dissolved in THF and re-precipitated in methanol (250 mL) to obtain the purified diblock copolymer (Supporting Information, Figure S1 and S2). Yield = 92%,  $M_n = 37\,000\text{ g mol}^{-1}$ , and PDI = 1.28 (GPC). Other diblock copolymers with different compositions were also synthesized

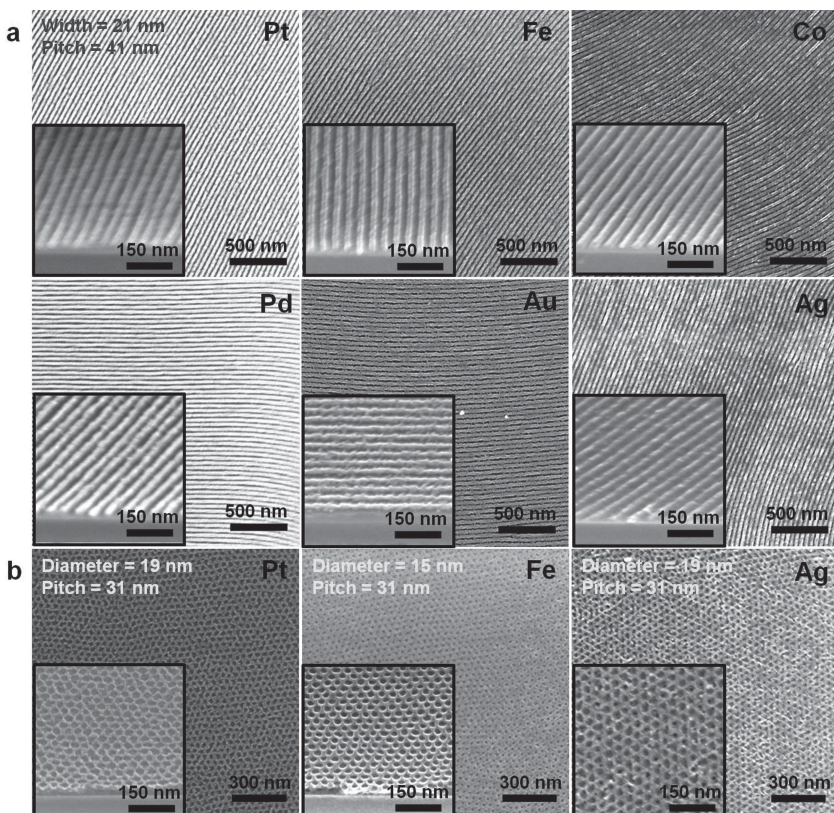


**Figure 6.** Various nanowires (a) and nanomeshes (b) fabricated from the M3BD47 and M4BD63 template, respectively. Metallic salt ions such as Pt, Fe, Co, Pd, Au, and Ag were selectively incorporated in the PDOPAM block, followed by O<sub>2</sub> plasma treatment for the removal of organic components. The plasma process partially oxidize the metals except Au, and thus a short thermal treatment under a reducing atmosphere (Ar/H<sub>2</sub>) is required to generate pure metallic nanostructures.

by changing the molar ratio of the crystalline DOPAM monomer to the PMMA-RAFT macroinitiator (Supporting Information, Scheme S1 and Table S3).<sup>[19]</sup>

**Preparation of Nanostructures from the Block Copolymer Thin Films:** The PMMA-*b*-PDOPAM diblock copolymer solutions in chloroform were spin-coated on a primitive silicon wafer (2 cm × 2 cm) or a SiO<sub>2</sub>(100nm)/Si wafer (silicon wafer coated with a 100 nm thick silicon oxide layer) by using a spin-coater (3000 rpm; 60 s). The film thickness was adjusted by controlling the solution concentration (0.5–1.0 wt%). The resulting thin films were put in a Petri dish (diameter = 10 cm) that was maintained under the vapor atmosphere of a mixed solvent of THF/cyclohexane = 8/2 (volume ratio), and then annealed for 24–48 h (humidity, 25 ± 3%) at room temperature to develop a nanostructure such as in-plane cylinder or square and/or hexagonal arrayed cylinder, dependent on the composition of PDOPAM in the block copolymer chains. After the solvent-annealing process, the PDOPAM blocks oriented in the annealed films were selectively stained by RuO<sub>4</sub>, exposed to UV (254 nm) for 15–20 min to decompose the PMMA blocks, immersed in 10 mL of 99.5% acetic acid solution for 20 min, taken out, and then washed with deionized water to remove the decomposed PMMA residual and the stained RuO<sub>4</sub> in the PDOPAM block.<sup>[19]</sup>

**Pattern Transfer by Reactive Ion Etching:** The prepared block copolymer nanotemplates were used as a mask for RIE to transfer the long-range-ordered line and space or well-defined hole patterns onto the underlying silicon dioxide layer. The CF<sub>4</sub>/Ar RIE process was carried out at conditions of power = 80 W, CF<sub>4</sub> flow rate = 60 sccm,

Ar flow rate = 20 sccm, pressure = 15 mTorr, and irradiation time = 120 s to etch the silicon oxide layer. After RIE, the films were treated with O<sub>2</sub> plasma (power = 50 W, flow rate = 40 sccm, pressure = 15 mTorr, and irradiation time = 60 s) to remove any remaining organic polymer templates.<sup>[19]</sup>

**Preparation of Nanowires or Naomeshes:** The prepared block copolymer nanotemplate films with in-plane cylindrical and hexagonally packed cylindrical morphologies were immersed in a desired aqueous metal salt solution, which was prepared by dissolving metal salts (Na<sub>2</sub>PtCl<sub>6</sub>, K<sub>3</sub>Fe(CN)<sub>6</sub>, K<sub>3</sub>Co(CN)<sub>6</sub>, Na<sub>2</sub>PdCl<sub>4</sub>, HAuCl<sub>4</sub>, or KAg(CN)<sub>2</sub>) of 20 mM to 30 mM in 3 mL of distilled water, in a Petri dish. After adsorption of the metallic cations on the amide groups in the side chain of the PDOPAM blocks for 3 h, the adsorbed film was thoroughly rinsed with a sufficient amount of distilled water to remove the freely remaining metallic cations and dried under a nitrogen stream. Finally, the oxygen plasma process was performed under a working pressure of 15 mTorr, a flow rate of 40 sccm, power of 50 W, and irradiation time of 60 s to decompose the PDOPAM blocks linked to the metallic cation polymer. During the oxygen plasma treatment, the adsorbed metal cations were converted into their oxides, except for gold metal, and are supported by their XPS data (Supporting Information, Figure S15). The thermal treatment of the metallic oxides with hydrogen gas at elevated temperature generates their corresponding metals. For example, when silver oxide (Ag<sub>2</sub>O) is heated at 300 °C for 1 min under a hydrogen atmosphere, it is reduced into pure Ag metal, as shown in Supporting Information, Figure S15.<sup>[32]</sup>

**Preparation of TEM Samples:** Cross-sectional TEM samples were prepared by focused ion beam (FIB) milling of the BCP films on a Si wafer. To

protect the BCP layer during the FIB milling process, a carbon layer was deposited on the surface of the films. TEM images were obtained using a JEOL JEM-ARM200F microscope operating at 200 kV.

## Supporting Information

Supporting Information is available from the Wiley Online Library or from the author.

## Acknowledgements

This research was funded by the Corporate R&D, LG Chem, Ltd., and also supported in part by the National Research Foundation of Korea (NRF) Grant (2010-0020973). The X-ray experiments at PAL were supported in part by MEST and POSTECH. The authors acknowledge Professor Sang Ouk Kim at KAIST for his valuable discussions. J.G.L. thanks financial support by a Seoul Science Fellowship through the Seoul Metropolitan Government and by Hanyang University.

Received: October 18, 2013

Revised: November 23, 2013

Published online:

- [1] G. M. Whitesides, B. Grzybowski, *Science* **2002**, *295*, 2418.
- [2] R. D. Piner, J. Zhu, F. Xu, S. Hong, C. A. Mirkin, *Science* **1999**, *283*, 661.
- [3] M. Park, C. Harrison, P. M. Chaikin, R. A. Register, D. H. Adamson, *Science* **1997**, *276*, 1401.
- [4] P. W. K. Rothemund, *Nature* **2006**, *440*, 297.
- [5] R. A. Segalman, H. Yokoyama, E. J. Kramer, *Adv. Mater.* **2001**, *13*, 1152.
- [6] S. O. Kim, H. H. Solak, M. P. Stoykovich, N. J. Ferrier, J. J. d. Pablo, P. F. Nealey, *Nature* **2003**, *424*, 411.
- [7] C. T. Black, R. Ruiz, G. Breyta, J. Y. Cheng, M. E. Colburn, K. W. Guarini, H. C. Kim, Y. Zhang, *IBM J. Res. Dev.* **2007**, *51*, 605.
- [8] I. Bita, J. K. W. Yang, Y. S. Jung, C. A. Ross, E. L. Thomas, K. K. Berggren, *Science* **2008**, *321*, 939.
- [9] K. G. A. Tavakkoli, K. W. Gotrik, A. F. Hannon, A. Alexander-Katz, C. A. Ross, K. K. Berggren, *Science* **2012**, *336*, 1294.
- [10] C. M. Bates, T. Seshimo, M. J. Maher, W. J. Durand, J. D. Cushen, L. M. Dean, G. Blachut, C. J. Ellison, C. G. Willson, *Science* **2012**, *338*, 775.
- [11] R. Ruiz, H. M. Kang, F. A. Detcheverry, E. Dobisz, D. S. Kercher, T. R. Albrecht, J. J. de Pablo, P. F. Nealey, *Science* **2008**, *321*, 936.
- [12] S. B. Darling, *Prog. Polym. Sci.* **2007**, *32*, 1152.
- [13] M. P. Stoykovich, M. Müller, S. O. Kim, H. H. Solak, E. W. Edwards, J. J. de Pablo, P. F. Nealey, *Science* **2005**, *308*, 1442.
- [14] S. Park, D. H. Lee, J. Xu, B. Kim, S. W. Hong, U. Jeong, T. Xu, T. P. Russell, *Science* **2009**, *323*, 1030.
- [15] J. K. W. Yang, Y. S. Jung, J.-B. Chang, R. A. Mickiewicz, A. Alexander-Katz, C. A. Ross, K. K. Berggren, *Nat. Nanotechnol.* **2010**, *5*, 256.
- [16] J. W. Jeong, W. I. Park, M.-J. Kim, C. A. Ross, Y. S. Jung, *Nano Lett.* **2011**, *11*, 4095.
- [17] D. J. C. Herr, *J. Mater. Res.* **2011**, *26*, 122.
- [18] S. H. Kim, M. J. Misner, T. Xu, M. Kimura, T. P. Russell, *Adv. Mater.* **2004**, *16*, 226.
- [19] Y. K. Han, J. G. Lee, S. H. Kim, (LG Chem), PCT WO 2012/144735, **2012**.
- [20] C. Barner-Kowollik, S. Perrier, *J. Polym. Sci. Polym. Chem.* **2008**, *46*, 5715.
- [21] Y. K. Han, J. G. Lee, J. S. Jeong, D. W. Sohn, S. H. Han, H. H. Song, K. M. Kim, (LG Chem), PCT WO 2012/057443, **2012**.
- [22] F. S. Bates, G. H. Fredrickson, *Annu. Rev. Phys. Chem.* **1990**, *41*, 525.
- [23] R. A. Segalman, *Mater. Sci. Eng. Rep.* **2005**, *R48*, 191.
- [24] V. P. Chuang, J. Gwyther, R. A. Mickiewicz, I. Manners, C. A. Ross, *Nano Lett.* **2009**, *9*, 4364.
- [25] C. Tang, E. M. Lennon, G. H. Fredrickson, E. J. Kramer, C. J. Hawker, *Science* **2008**, *322*, 429.
- [26] S.-M. Park, G. S. W. Craig, Y.-H. La, H. H. Solak, P. F. Nealey, *Macromolecules* **2007**, *40*, 5084.
- [27] J. Bang, S. H. Kim, E. Drockenmuller, M. J. Misner, T. P. Russell, C. J. Hawker, *J. Am. Chem. Soc.* **2006**, *128*, 7622.
- [28] K. H. Kim, Y. G. Kim, Y. Kwon, *Macromol. Res.* **2009**, *17*, 388.
- [29] P. F. Green, T. M. Christensen, T. P. Russell, R. Jérôme, *Macromolecules* **1989**, *22*, 2189.
- [30] R. Ruiz, J. K. Bosworth, C. T. Black, *Phys. Rev. B* **2008**, *77*, 054204.
- [31] As a reference for other nanofabrication processes, etch selectivity between PDOPAM and PMMA without staining is  $2.0 \pm 0.2$  under  $O_2$  plasma generated with a power of 50 W and a working pressure of 15 mTorr.
- [32] Y. K. Han, J. G. Lee, H. J. Lee, N. M. Kim, S. S. Yoon, E. J. Shin, (LG Chem), Korea 10-2012-0116608, **2012**.
- [33] J. Chai, D. Wang, X. Fan, J. M. Buriak, *Nat. Nanotechnol.* **2007**, *2*, 500.
- [34] T. H. Reilly, R. C. Tenent, T. M. Barnes, K. L. Rowlen, J. van de Lagemaat, *ACS Nano* **2010**, *4*, 615.
- [35] a) Q. Peng, Y. C. Tseng, S. B. Darling, J. W. Elam, *Adv. Mater.* **2010**, *22*, 5129; b) Q. Peng, Y. C. Tseng, S. B. Darling, J. W. Elam, *ACS Nano* **2011**, *5*, 4600.